Engineering Applications of Computational Fluid Mechanics Vol. 6, No. 2, pp. 173–185 (2012)

NUMERICAL SIMULATION OF AERODYNAMIC NOISE GENERATED BY HIGH SPEED TRAINS

Zhenxu Sun **, Jingjing Song [#] and Yiran An *

** State Key Laboratory for Turbulence and Complex Systems, College of Engineering, Peking University, Beijing 100871, China*
E-Mail: anyr@pku.edu.cn (*Corresponding Author*)
*** State Key Laboratory of High Temperature Gas Dynamics, Institute of Mechanics, Academia Sinica, Beijing 100190, China*
[#] China Academy of Aerospace Aerodynamics, Beijing 100074, China

ABSTRACT: Aerodynamic noise becomes more and more significant and sometimes could be predominant as the running speed of high speed trains increases. As a result, aerodynamic noise has to be taken into consideration during the design of high speed trains. In present work, the research on aerodynamic noise of the high speed train with a speed of 300 km/h has been performed. The nonlinear acoustics solver (NLAS) approach is adopted to study the aerodynamic noise in the near field of the high speed train. With the use of an acoustic surface, the research on the aerodynamic noise in the far field has been carried out by solving the Ffowcs-Williams/Hawking (FW-H) equation. At first the method validation is performed through a two-dimensional backward step case, which shows excellent agreement with experimental results. The characteristics of the flow field dominate the generation of aerodynamic noise, therefore the flow field is firstly analyzed, including the head, the rear, and the inter-coach spacing of the train. By use of probes in specific regions on the surface of the train, the contribution of different parts of the train to the aerodynamic noise is discussed. Meanwhile, the far field feature of aerodynamic noise is also studied by placing probes in the far field. Based on the above analysis, the aerodynamic noise performance of the specific high speed train is assessed.

Keywords: high speed trains, aerodynamic noise, NLAS, FW-H equation, acoustic surface

1. INTRODUCTION

Environmental problems induced by trains' noise remain a key issue during the development of high speed trains. The standards of environmental quality for the noise of high speed trains are implemented in many developed countries and regions such as Japan and the European Union. The noise level of newly designed high speed trains should meet the standards (Kitagawa and Nagakura, 2000; Pronello, 2003; Kalivoda et al., 2003). With the increase of the running speed of high speed trains and the raise of requirement for environmental quality, the standards are set higher and higher. In the meantime, the high speed railway in China is experiencing a booming stage, so the noise study is much more urgent and detailed research should be performed from the very beginning.

Basically, the study on the noise of high speed trains focuses on the study of noise sources, including the location and clarification of noise sources (Talotte et al., 2003). In general, the noise of high speed trains could be categorized into two kinds: rolling noise and aerodynamic noise. The former mainly refers to mechanical noise, generated by wheel vibration and rail vibration. Study on Shinkansen trains in Japan reveals that rail noise contributes the major part for rolling noise (Moritoh et al., 1996). This conclusion is mainly based on the following observations: the frequency spectrum of wheel vibration is significantly different from the sound spectrum measured under the floor of the running train. However, the rail vibration velocity has the same spectrum as that of the sound measured near the rail when the train runs over it at frequencies greater than 500Hz. An efficient way to reduce this kind of rolling noise is to improve the adhesion between wheels and rail, which has been very successful nowadays. The latter is mainly induced by the specific flow structures in the flow field. Moreover, only the noise directly radiated by the vibration of train surfaces is considered. Two kinds of noise sources are specified (Talotte, 2000): one is that radiated by the steady flow structures. For example, the steady vortex shedding just behind the pantograph can generate significant aerodynamic noise, which contributes a major part of the noise. Besides, some cavity

Received: 5 Apr. 2011; Revised: 2 Nov. 2011; Accepted: 19 Nov. 2011

structures on the surface of high speed trains can also generate aerodynamic noise (Noger et al., 2000). For example, the inter-coach spacing and the recess of pantograph on TGV high speed trains in France are both cavity noise sources. The other one is that emitted by turbulent fluctuations, which mostly locates in the turbulent boundary layer around the surface of high speed trains or in places where flow separations take place.

As the speed of high speed trains increases, the contribution from rolling noise and aerodynamic noise changes (Mellet et al., 2006). The sound power of aerodynamic noise increases with the sixth order of the running speed, indicating that the aerodynamic noise must not be ignored when the train runs at a high speed. At low speeds (usually less than 250 km/h) the rolling noise is slightly predominant while when the train runs at speed above 300 km/h the aerodynamic noise becomes the major part. As a result, when the train is running at a high speed, the overall noise level can never be reduced if the reduction of mechanical noise is considered alone. In this situation the aerodynamic noise must be taken into consideration.

Currently the study on aerodynamic noise of high speed trains mainly includes experiments and numerical approaches. The former can be specified into two kinds, namely the real vehicle tests and wind tunnel investigations on scaled models (Mellet et al., 2006; Nagakura, 2006). Real vehicle tests suffer from a long time period and too much input for manpower and material resources. Wind tunnel investigations always suffer from the conditions that scaled models has to be compatible with the prototype in geometry and flow conditions (such as Reynolds number and turbulent intensity of boundary layer). On the other hand, with the development of modern computers, numerical simulations are gradually accepted to predict the aerodynamic noise. Compared to experiments, numerical simulation benefits include a relatively short computational period, the flexibility to control flow conditions and the feasibility to simulate cases in extreme conditions which could not be met frequently in normal life. However, both the wind tunnel investigations and numerical simulations suffer from the credibility problem, so that the method validation must be performed before the method could be employed.

The method to numerically simulate the aerodynamic noise varies a lot with the computational algorithms. Currently two commonly used methods exist in computational aero-acoustics. The first one is direct simulation, including direct numerical simulation (DNS), large eddy simulation (LES), and unsteady RANS (URANS) simulation. DNS and LES have a massive requirement for grids, which greatly limits its applications to engineering problems. For example, in order to capture noise sources with high frequencies, DNS requires grids with an amount of $Re^{9/4}$, which is a great challenge to modern computers. On the contrary, URANS could satisfy the need for grids in engineering problems, but it could bring a relatively large numerical error due to its failure in capturing the sources in sub-grid scales. The second approach is the acoustic analogy methods. It was originated by Lighthill who derived the well known Lighthill equation (Lighthill, 1952 and 1954). But it is a volume integral method, which unfortunately limits its applications. Later on, Curle (1955) solved the Lighthill equation within a solid boundary. Then Ffowcs-Williams and Hawkings extended Curle's solution to the moving boundary, and derived the famous FW-H equation (Williams and Hawkings, 1969). It is a surface integral method which is much more applicable. It assumes that sound propagation follows the simple wave equation and could be solved through the integration on the surface surrounding the nonlinear acoustic sources. Casper and Farassat (2002a and 2002b) have done a thorough research on FW-H equation and a lot of formulas have been obtained. This approach has an obvious advantage in predicting far field noise due to its ignorance in mesh resolution for far field probes and even more the far field probes need not be in the computational domain.

In present work, numerical simulation of aerodynamic noise generated by a specific high speed train has been conducted. Because both near field noise and far field noise are concerned here, the mesh problem becomes critical and proper computational approaches have to be selected cautiously. The nonlinear acoustics solver method (NLAS), which is derived by Batten et al. (2002 and 2004), has been chosen to solve the near field aerodynamic noise. It is a nonlinear method and its requirement for grids can be relaxed on the near wall. Reconstruction of turbulence variables takes the sub-grid sources into consideration, which could both reduce the grid requirement and maintain the computational accuracy. Meanwhile, in order to accurately predict the far field noise, an acoustic surface is built around the high speed train to record pressure fluctuations. Then the study on far field noise is performed by solving the FW-H equation.

2. ALGORITHMS

Two kinds of approaches are adopted in present work, NLAS to solve the near field noise and FW-H sound propagation method to solve the far field noise. For the latter approach, an acoustic surface around the noise sources is built to record fluctuation data during NLAS calculation, which would be taken as the initial value for FW-H propagation equation. The overall solving process is shown in Fig. 1:

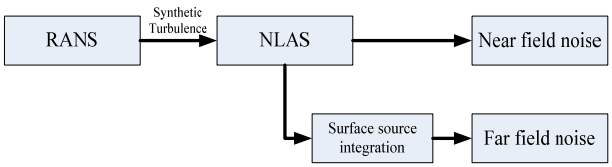

Fig. 1 Schematic drawing of solution procedure

2.1 Nonlinear acoustics solver

The basic concept of NLAS is that aerodynamic noise sources emitted by turbulence in sub-grid scales have to be modeled. Meanwhile, noise sources in middle and large scales, such as cavities, are also modeled by this method (Batten et al., 2002 and 2004).

The NLAS is a numerical acoustics solver designed to model noise generation and propagation from an initial statistically-steady model of turbulent flow data, which can be provided by a simple RANS model. The statistical steady RANS data provides a baseline description of the mean flow as well as a statistical description of the superimposed turbulent fluctuations. The NLAS then uses a reconstruction procedure to generate noise sources from the given set of statistics and allows the resulting propagation of the pressure disturbances to be simulated using a high resolution pre-conditioned solver.

Moreover, NLAS is a low diffusion solver and can model the generation of noise in sub-grid scales. It relies on the concept that sub-grid noise can be obtained by statistical models through a priori mean-flow computation. Perturbation is assumed to be added into NS equations in NLAS, in which quantities are split into mean and fluctuating parts. Substituting into the NS equations and rearranging for fluctuation and mean quantities gives a system of perturbation equations referred to as non-linear disturbance equations (NLDE):

$$\frac{\partial Q'}{\partial t}+\frac{\partial F_i'}{\partial x_i}-\frac{\partial (F_i^{\upsilon})'}{\partial x_i}=-\frac{\partial \overline{Q}}{\partial t}-\frac{\partial \overline{F}_i}{\partial x_i}+\frac{\partial \overline{F}_i^{\upsilon}}{\partial x_i} \tag{1}$$

$$\overline{Q}=\begin{bmatrix}\overline{\rho}\\ \overline{\rho u}_j\\ \overline{e}\end{bmatrix},\overline{F}_i=\begin{bmatrix}\overline{\rho u}_i\\ \overline{\rho u}_i\overline{u}_j+\overline{p}\delta_{ij}\\ \overline{u}_i(\overline{e}+\overline{p})\end{bmatrix},\overline{F}_i^{\upsilon}=\begin{bmatrix}0\\ \overline{\tau}_{ij}\\ -\overline{\theta}_i+\overline{u}_k\overline{\tau}_{ki}\end{bmatrix} \tag{2}$$

$$Q'=\begin{bmatrix}\rho'\\ \overline{\rho}u_j'+\rho'\overline{u}_j+\rho'u_j'\\ e'\end{bmatrix}, \tag{3}$$

$$\left(F_i^{\upsilon}\right)'=\begin{bmatrix}0\\ \tau_{ij}'\\ -\theta_i'+u_k'\overline{\tau}_{ki}+\overline{u}_k\tau_{ki}'\end{bmatrix}$$

$$F_i'=\begin{bmatrix}\overline{\rho}u_i'+\rho'\overline{u}_i\\ \rho'\overline{u}_i\overline{u}_j+\overline{\rho}\overline{u}_iu_j'+\overline{\rho}u_i'\overline{u}_j+p'\delta_{ij}\\ u_i'(\overline{e}+\overline{p})+\overline{u}_i(e'+p')\end{bmatrix}+ \tag{4}$$

$$\begin{bmatrix}\rho'u_i'\\ \overline{\rho}u_i'u_j'+\rho'u_i'\overline{u}_j+\rho'\overline{u}_iu_j'+\rho'u_i'u_j'\\ u_i'(e'+p')\end{bmatrix}$$

Neglecting density fluctuations and taking time averages gives:

$$\overline{LHS}=\overline{RHS}=\frac{\partial R_i}{\partial x_i} \tag{5}$$

$$R_i=\begin{bmatrix}0\\ \overline{\rho}\overline{u_i'u_j'}\\ c_p\overline{\rho T'u_i'}+\overline{\rho}\overline{u_i'u_k'}\overline{u}_k+\frac{1}{2}\overline{\rho}\overline{u_k'u_k'u_i'}+\overline{u_k'\tau_{ki}}\end{bmatrix} \tag{6}$$

The above terms correspond to the standard Reynolds-stress tensor and turbulent heat fluxes. The key step in NLAS is to obtain these unknown terms in advance from a classical RANS method. Subsequently, a synthetic reconstruction of the un-resolvable contribution to these terms can then be generated and used to form the sub-grid source terms for the NLAS simulation.

NLAS provides a more sophisticated sub-grid treatment that allows the extraction of acoustic sources from the temporal variation within the sub-grid structures. The dissipative effects of a sub-grid eddy viscosity model are avoided, thus, on coarser meshes, NLAS proves less diffusive than LES.

2.2 FW-H equation

The acoustic surface is used to record fluctuation data during the NLAS procedure. Once the data is obtained, Ffowcs-Williams/Hawking equation can be solved on the basis of these data. The FW-H equation approach can be used to predict any observation point outside the acoustic surface, even if the observation point is outside the computational domain. The basic form of Ffowcs-Williams/Hawking equation takes the form as:

$$\begin{aligned} &4\pi p'(x_i,t) \\ &= \iint\left[\frac{\dot{Q}_j\hat{n}_j}{r(1-M_r)^2}+\frac{Q_j\hat{n}_j(r\dot{M}_r+c_\infty(M_r-M^2))}{r^2\left|1-M_r\right|^3}\right]_{ret} ds \\ &+\iint\left[\frac{\dot{L}_j\hat{r}_j}{c_\infty r(1-M_r)^2}+\frac{L_j\hat{r}_j-L_jM_r}{r^2(1-M_r)^2}\right]_{ret} ds \\ &+\iint\left[\frac{L_j\hat{r}_j(r\dot{M}_r\hat{r}_k+c_\infty(M_r\hat{r}_k-M^2))}{c_\infty r^2\left|1-M_r\right|^3}\right]_{ret} ds+p'_Q \end{aligned} \tag{7}$$

in which

$$\begin{aligned} Q_i &= (\rho_\infty-\rho)v_i+\rho u_i \\ L_i &= p\hat{n}_i+\rho u_i(u_j-v_j)n_j \end{aligned} \tag{8}$$

2.3 Turbulence model

Statistically steady RANS calculation is required before the NLAS calculation. The main generation zone for turbulence, which would usually become the relatively steady noise sources in the flow field, can be obtained by RANS calculation. Meanwhile, a statistically steady mean flow could be prepared by RANS calculation. In order to preferably model the statistically steady flow field, an anisotropic turbulence model, the cubic $k-\varepsilon$ model (Merci et al., 2001), is utilized in present paper. This model has non-linear terms accounting for normal-stress anisotropy, swirl and streamline curvature effects, so that the best description of the local Reynolds-stress tensor can be provided, which is subsequently used to synthesize the noise sources.

3. METHOD VALIDATION

A two-dimensional backward step case is chosen as the test case here. It comes from the experiment in literature (Lee and Sung, 2001), which was carried out in a subsonic wind tunnel. The flow conditions in the numerical simulation are the same as those of the experiment. In the experiment the spanwise width is 12.5 times of the height of the backward step so as to keep the central section two-dimensional. As a result, a two-dimensional simulation has been conducted for the central section in this paper. The observation points are chosen just on the floor behind the step, as the experiment did. FFT analysis is performed on the fluctuating pressure data. Meanwhile, numerical simulation with the LES approach is also performed. The results from the NLAS approach, the LES approach and the experiment are listed together for comparison, which mainly focuses on the sound pressure level and corresponding dominant frequency.

The details of the numerical simulation can be referred to Sun et al. (2010), and here only the comparison of sound pressure level and dominant frequency among different approaches are listed in Tables 1 and 2.

Table 1 Maximal sound pressure level (dB, x is distance from probe to step and H is height of step).

	x/H=2	x/H=4	x/H=6	x/H=8	x/H=10
Experiment	-26	-27	-24.2	-22.6	-24
NLAS	-26	-23	-24.35	-21.7	-23.2
LES	-26.27	-25.2	-23.04	-18.6	-19.54

Table 2 Dominant frequency (Hz, x is distance from probe to step and H is height of step).

	x/H=2	x/H=4	x/H=6	x/H=8	x/H=10
Experiment	11.5	10.5	18	12	18
NLAS	14	7.1	13	13	9.1
LES	13.9	14.5	28.5	28.5	43

As presented in the Tables 1 and 2, better dominant frequencies are achieved through the NLAS approach, except for the position x/H=10. Meanwhile, the maximal sound pressure level predicted by NLAS agrees well with the experimental data. However, the maximal sound pressure level and dominant frequency obtained by LES under the same mesh and flow conditions show relatively more variation with experimental data. This can be related to that the synthetic reconstruction of sub-grid sources can be achieved in NLAS approach rather than LES approach, which makes the results from NLAS approach more accurate. Simulation results reveal that the NLAS approach is an efficient and high-resolution computational method for aerodynamic noise prediction, and can be adopted for the large scale computation of aerodynamic noise generated by high speed trains.

4. RESULTS AND DISCUSSION

4.1 Computational model and mesh

Simulation of aerodynamic noise generated by the high speed train is performed in this paper, and the acoustic influence from the streamline shape of the train is the main concern, so that the pantograph and the bogie area are all neglected. Three coaches are considered, including a leading car, the middle coach and a rear power car, as Fig 2 shows. The ground just locates below the train. The whole computational domain is 375m long and 150m wide, taking the shape of a semi-cylinder, as shown in Fig. 3.

The near wall grids for aerodynamic noise prediction must be fine enough to capture high frequency sources. The number of grids is about 10.34 million, and specific regions such as the nose of the power car are densified to preferably capture the flow details with large gradient variations, as Fig 4 shows. Meanwhile, the area inside the acoustic surface is also densified to maintain the accuracy of fluctuating data. 15 prism layers are built just around the surface of the high speed train with a 1.1 stretching ratio, and the initial distance of the grids is set to 2.5e-4m. Considering the unsteady rear flow behind the high speed train, the acoustic surface is distinctly longer than the train. The acoustic surface is shown in Fig. 5.

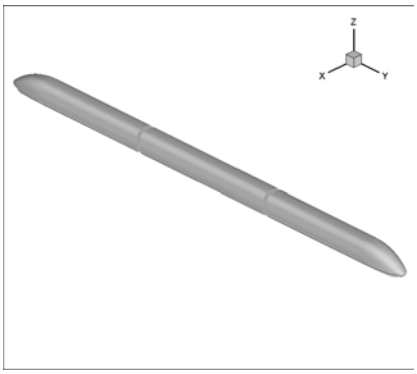

Fig. 2 Geometry of high speed train.

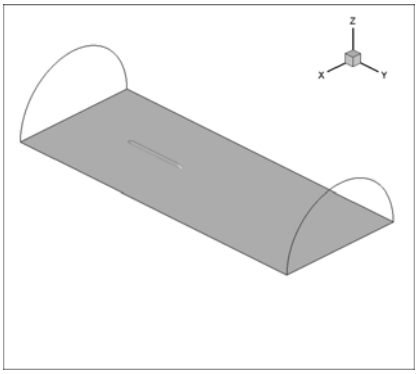

Fig. 3 Whole domain.

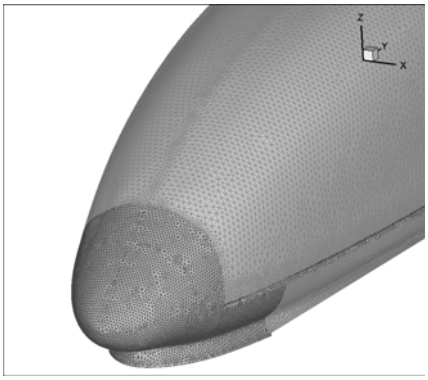

Fig. 4 Mesh around nose of power car.

Fig. 5 Acoustic surface.

4.2 Probes configuration

The main purpose of this paper is to study the aerodynamic noise induced by the train's body and inter-coach spacing, and thus the following locations are specifically chosen to place probes:

1. the nose of the leading car, which is a stagnation zone. Flow around here experiences a sudden change in gradient and complex flow phenomena such as flow transition and separations may take place. The specific locations are shown in Figs. 6 and 7.
2. top and side of the coaches, where turbulent boundary layer may vary significantly. The specific configuration on these places is shown in Fig. 8.
3. the inter-coach spacing, where cavity flow and acoustic resonances (Fremion et al., 2000) may occur. The specific configuration on these places is shown in Fig. 9.
4. the nose of the rear power car, where strongly unsteady flow exists. The specific configuration on these places is shown in Fig. 10.
5. for the prediction of far field noise, a unified standard is utilized here (25m away and 3m high). The specific configuration on these places is shown in Fig. 11.

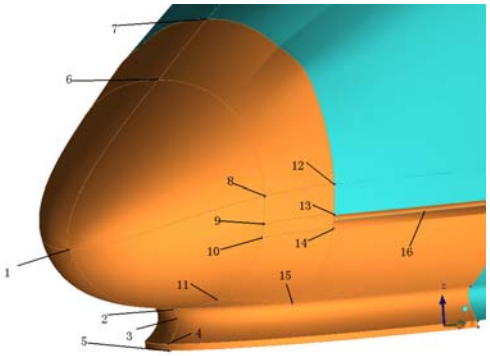

Fig. 6 Probes configuration on nose of the leading car.

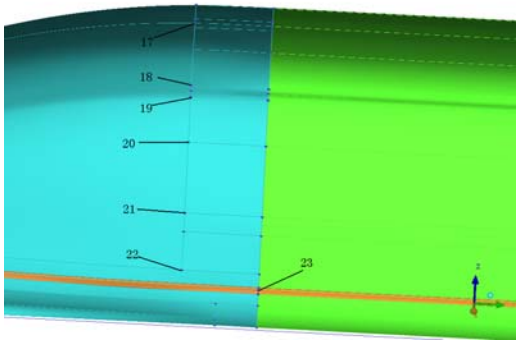

Fig. 7 Probes configuration on head of leading car.

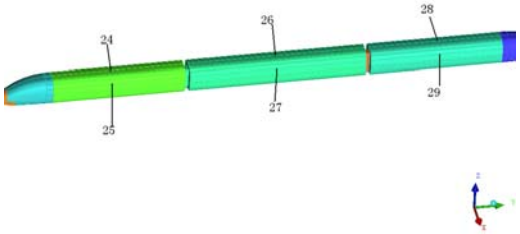

Fig. 8 Probes configuration on top and side of coaches.

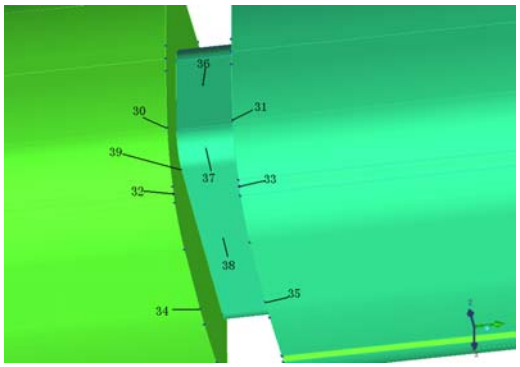

Fig. 9 Probes configuration in inter-coaching spacing.

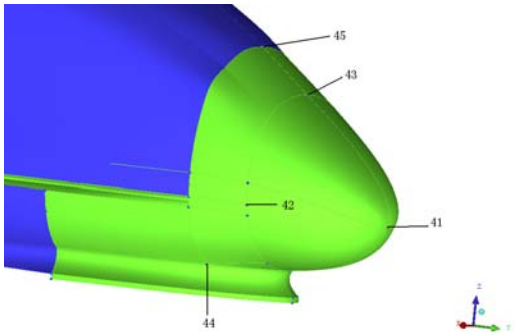

Fig. 10 Probes configuration on nose of rear power car.

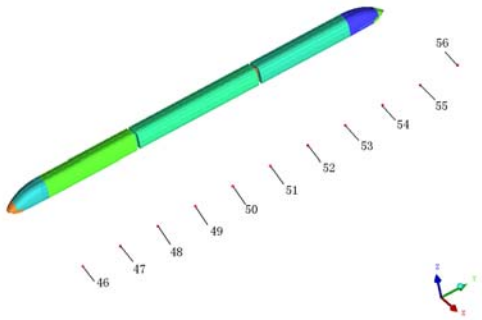

Fig. 11 Probes configuration in far field.

4.3 Flow conditions

When statistically steady RANS calculation is performed, a uniform velocity flow condition is utilized with a speed of 300 km/h at the inlet boundary, and the ground is set to be a moving wall with the same speed as the inlet boundary. A pressure outlet condition is imposed at the outlet boundary with a 0 Pa gauge pressure. The reference pressure is set to be 1 atm. When the NLAS procedure is conducted, one absorbing layer is imposed on the inlet boundary, the outlet boundary and the far field boundary to prevent wave reflections from these boundaries. 200 Fourier modes are set to perform synthetic reconstruction for the turbulent fluctuating quantities so as to capture the sub-grid sources correctly. The time step in NLAS simulation is set to 2e-5s, and the simulated physical time is 0.3s, so as to insure that the noises whose frequency locate between 10-10000Hz could be precisely predicted.

4.4 Analysis of flow field

The flow field obtained by RANS calculation is a statistical field, in which all the quantities are statistical results based on turbulent fluctuations. As a complex, slender and fast moving object above the ground, the high speed train would

generate a complex turbulent flow, which interacts with a number of structural elements. Flow analysis on specific parts of the train will be shown in the sections below.

4.4.1 Head of the power car

The head of the high speed train has a perfect streamline shape, which would benefit a lot from reducing the drag and aerodynamic noise induced by the power car. Figs. 12 and 13 show the pressure contours and turbulent intensity contours of the power car, respectively.

The velocity is zero at the stagnation point on top of the nose, while the pressure rises to maximum and the turbulent intensity is zero here. After coming across the stagnation zone, the flow gets accelerated, accompanied with a decreasing pressure. The turbulent intensity begins to rise, revealing that the flow begins to be turbulent. Further investigation reveals that the region below the fairing experiences relatively high turbulent intensity, indicating that flow separation occurs here, which makes the flow more turbulent.

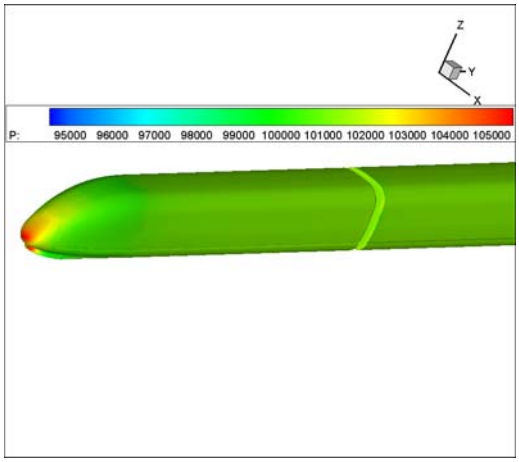

Fig. 12 Pressure contours of power car.

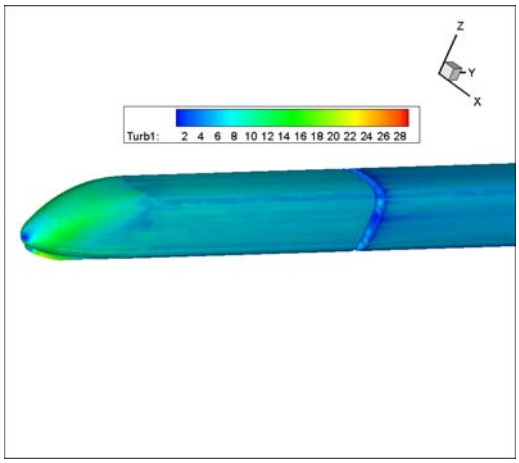

Fig. 13 Turbulent intensity contours of power car.

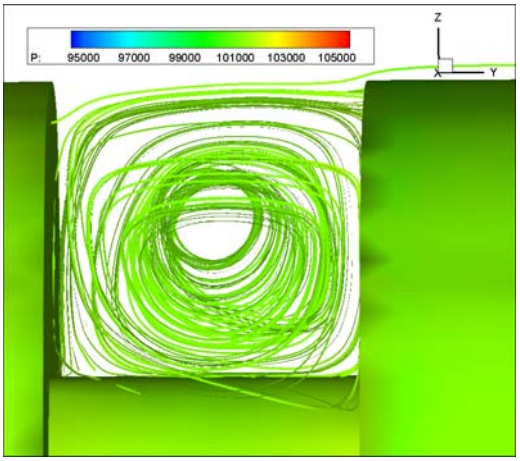

Fig. 14 Streamlines in inter-coach spacing-1.

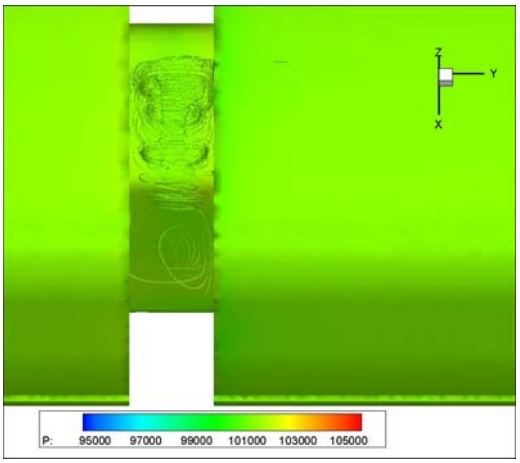

Fig. 15 Streamlines in inter-coach spacing -2.

4.4.2 Inter-coach spacing

Observation on the inter-coach spacing of the high speed train reveals that the cavity here has a 1:1 ratio of length to height, which seems to be an 'open cavity'. However, considering that the length of the inter-coach spacing is limited and open area exists on both sides of the cavity, thus the flow in the inter-coaching spacing cannot be seen as an open cavity. Compared to the latter, the flow in the inter-coach spacing shows a very complicated three-dimensional effect. Streamlines in the inter-coach spacing are depicted in Figs. 14 and 15.

As the above figures show, a big vortex emerges just on top of the surface in the x-coordinate (axial) direction. After coming across the surface, the swirl flow turns downward, and the major vortex turns into the z-direction, which makes the whole region turbulent, resulting in a high sound pressure level. The flow upstream separates from the leading edge of the inter-coach spacing and a strong shear layer then forms. Due to the relatively short length to height ratio, the inter-coach spacing could be treated as an open cavity,

such that the shear layer could extend to the trail edge and interacts with the boundary layer there. Driven by the upper shear layer, the flow in the inter-coach spacing experiences a much more turbulent flow and forms the large vortex which stretches along the surface of the spacing.

4.4.3 Train wake

Distinct difference exists between the flow around the leading car and the flow in the rear region. Flow in the rear region turns out to be more irregular due to the disturbance from the head and the body of the train. Figure 16 shows the pressure contour on the rear car and Figs. 17 and 18 show the streamlines around the rear car. Meanwhile, streamlines around the leading car are also depicted in Fig. 19 for comparison, in which the streamlines are colored by pressure.

As Fig 16 shows, a high pressure zone also exists on the tip of the rear nose, but is very smaller than the high pressure zone on the head of the leading car. As Figs. 17 and 18 show, the streamlines in the rear region seem more irregular and the flow here has a relatively large turbulent intensity. Two big vortices could be found stretching backward with opposite swirling directions. Although the precise nature of the wake varies from vehicle to vehicle, there seem to be a relatively small number of flow mechanisms that exist in common: shear layer separations, longitudinal helical flows, vortex streets and a separation cavity. All of these phenomena are subject to instabilities with Strouhal numbers. It can be seen in Figs. 17 and 18 that there is strong evidence of helical vortices behind the train, which extend a considerable distance into the rear region. Better results could be obtained by an unsteady simulation. However, since the purpose of the calculation of the flow field is to obtain its statistical characteristics, a steady RANS calculation suffices. Investigation on the streamlines in Fig 19 reveals that uniform streamlines come from the upwind region and then extend to both sides of the body. A regular vortex can be observed just between the nose and the fairing, which then stretches along lateral

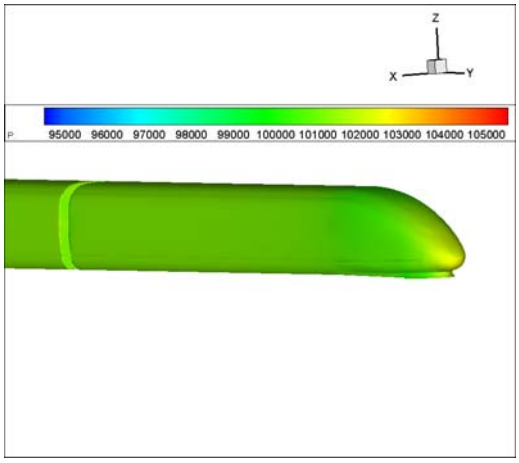

Fig. 16 Pressure contours of rear power car.

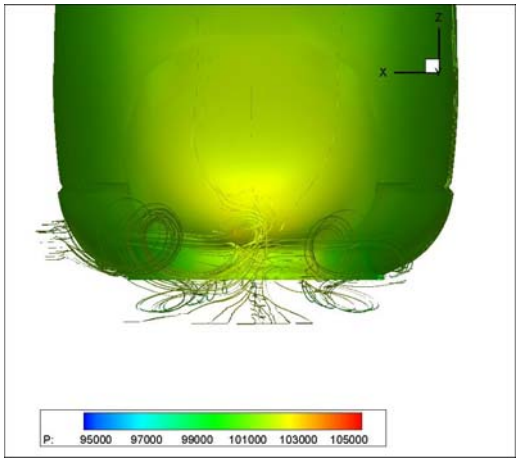

Fig. 17 Streamlines around rear power car (colored by pressure) -1.

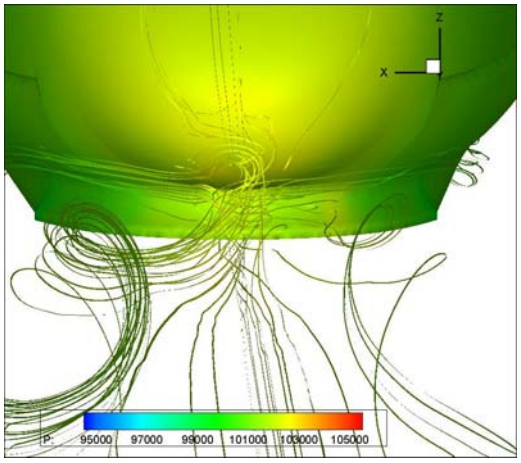

Fig. 18 Streamlines around rear power car (colored by pressure) -2.

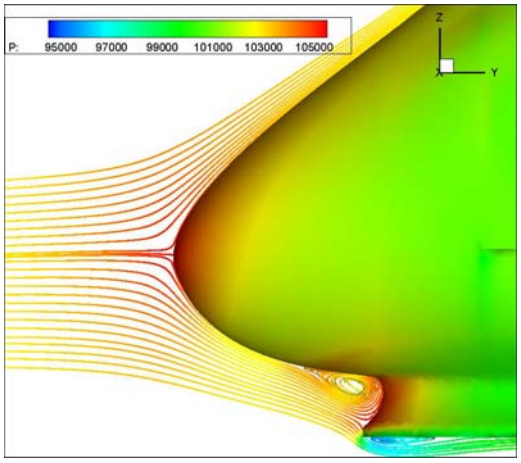

Fig. 19 Streamlines around leading car (colored by pressure).

sides of the train. Flow separation does not occur on top of the nose due to its perfect streamline shape. However, flow separation could be easily discovered just below the fairing, which confirms the previous turbulent intensity discussion.

4.5 Analysis of aerodynamic noise

Based on the statistical results obtained by RANS simulation, synthetic reconstruction of turbulent quantities can be accomplished by NLAS approach, which could be used to predict aerodynamic noise. Near field noise could be directly obtained through these fluctuating variables with the FFT tool. Meanwhile, these fluctuating quantities are also recorded on the acoustic surface, acting as the sources for far field noise. When the data on the acoustic surface is obtained, FW-H equation then could be solved to predict far field noise. Both near field and far field noise are obtained in this work, which will be analyzed in details in the following sections.

4.5.1 Head of power car

The probe P01 locates just on top of the nose of the power car, and exhibits some difference in the pattern of frequency spectrum of A-weighted sound pressure compared with those of other near field probes. As an example, probe P41, which locates in the rear stagnation region, is chosen for comparison. P01 and P41 are in similar positions of the leading and rear cars. Frequency spectrums of A-weighted sound pressure of P01 and P41 are shown in Figs. 20 and 21.

As Fig. 20 shows, the dominant frequency of P01 is about 2059Hz, indicating that this position is a high frequency noise source compared to the other probes. Meanwhile, except for the dominant frequency, other frequency modes are also observed, which are all above 1000Hz. The energy-contained frequencies mainly gather in the middle and high bands. However, P41 produces a broad-band noise, with its dominant frequency locating around 100Hz. The noise energy of P41 mainly locates in the band before 1000Hz. Study on the A-weighted sound pressure level of the two probes reveals that the noise energy contained in the rear of the train is greatly large than that contained in the leading car, implying that greater environmental damage could be done by the rear car than the leading car.

In addition to the stagnation point P01 in the leading car, another stagnation point P03 also exists in the place just between the nose and the fairing. Comparing the frequency spectrums of these stagnation points, observation could be

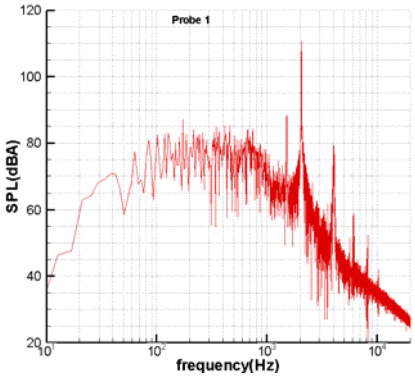

Fig. 20 Frequency spectrum of A-weighted sound pressure of P01.

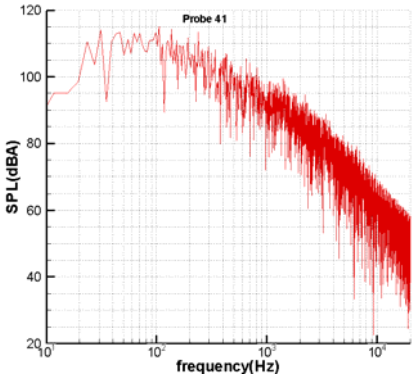

Fig. 21 Frequency spectrum of A-weighted sound pressure of P41.

made that P03 produces an A-weighted sound pressure level of 124.5 dB(A), apparently higher than that of probe P01, whose level is 110.7 dB(A). It can be attributed to the vortex stretching along the surface in the concave zone, which could enlarge the turbulent intensity and flow fluctuations. Two probes (P11 and P15), locating on the place where this vortex passes through, also generate high level noise.

Investigation has also been performed on probes P17, P18, P19 and P20. P17 and P20 are just on top of the leading car, while P18 and P19 are on the shoulder area of the leading car, where great curvature occurs. Results show that the probes on the shoulder generate greater noise level than the other two. The main noise sources around the surface of the train are boundary layer. Severe turbulence or flow separation in the boundary layer could lead to a bigger noise level. As the results show, the region on top of the nose has a smooth flow, while the shoulder area experiences a much more turbulent flow due to its great curvature. This sheds lights on the design of high speed trains that sharp transition between the surfaces should be avoided and the connection between adjacent parts should be made smoothly to smooth the flow and reduce the noise.

4.5.2 Inter-coach spacing

The flow in the inter-coach spacing is similar to the cavity flow, however it should not be simply treated as a cavity flow. Open area exists on both sides of the spacing, making the flow here more complicated. Three probes, P30, P32 and P34, are placed on the leading surface of the spacing, among which the highest A-weighted sound pressure level is 113.9 dB(A); three probes, P36, P37 and P38, are placed just on the middle of the spacing, with a highest noise level of 116.9 dB(A); another three probes, P31, P33 and P35, are placed on the trailing surface of the spacing, among which the highest sound pressure level is 121.5 dB(A). As the above results show, the downstream area generates the biggest noise in the inter-coach spacing zone, indicating that the trailing surface of the inter-coach spacing is the main noise source. It can be related with the strong shear layer generated by flow separation from the leading edge. When the shear layer interacts with the boundary layer on the trailing surface, stronger noise then can radiate from the trailing surface. Meanwhile, the noise generated in the connection surface is mainly attributed to the complicated vortex there.

Besides, two flutes exist just behind the streamline head of the high speed train, which could be used to stabilize the flow. Calculation of aerodynamic noise around these places reveals that stronger noise could be generated due to these flutes. Noise comparison of places in and out of the flutes is performed. For example, probes P14 and P23 are in the flutes while probes P13 and P22 which are adjacent to P14 and P23, are just placed in the smooth area outside the flutes. Frequency spectrums of A-weighted sound pressure of these probes are shown in Figs. 22 to 25.

As the figures show, in general, the probes inside the flutes generate stronger noise than the adjacent smooth area outside the flutes, and are higher with an noise level of 5-10 dB(A). It can be deduced that uneven surfaces of the train usually generate higher noise. For example, parts such as windows and doors that are not flush with the surface of the train are also noise sources, which could not be neglected.

4.5.3 Coach and rear power car

Six probes, probes P24 to P29, are placed on top and side of the coaches, and the highest noise level is found on probe P26, with a value of 113.7 dB(A). Compared to the other locations, these

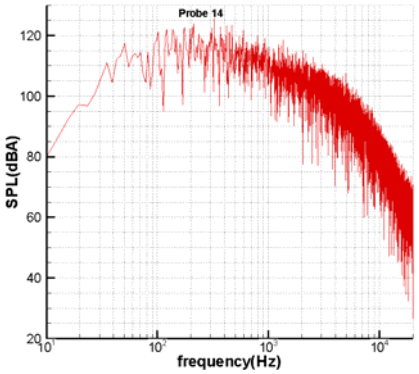

Fig. 22 Frequency spectrum of A-weighted sound pressure of P14.

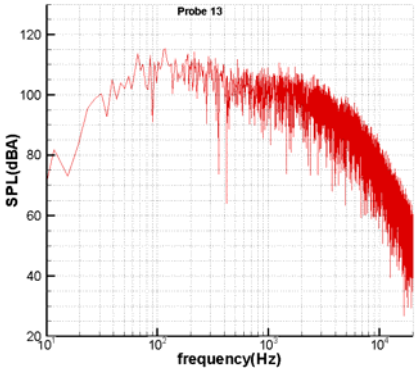

Fig. 23 Frequency spectrum of A-weighted sound pressure of P13.

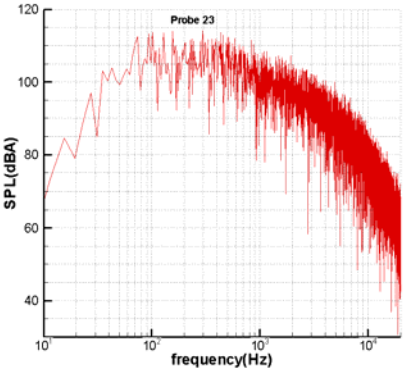

Fig. 24 Frequency spectrum of A-weighted sound pressure of P23.

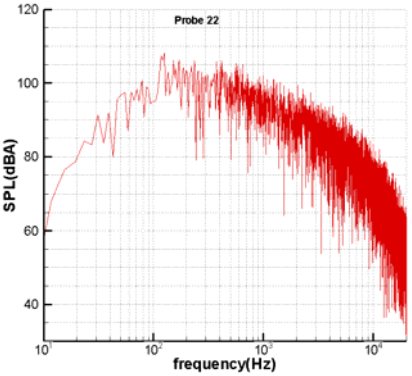

Fig. 25 Frequency spectrum of A-weighted sound pressure of P22.

smooth surface and undisturbed flow. Consequently, these places are not main noise sources.

Investigation on the noise induced by the rear power car is mainly through the comparison with similar places on the leading power car. For the rear stagnation point P41, its noise level is about 115.1 dB(A), while the corresponding probe in the leading car P01 has a level of 110.7 dB(A). The probe on top of the nose of the rear car, P43, generates noise with a level of 109.5 dB(A), while the corresponding probe in the leading car P06 has a level of 105.2 dB(A). Similar phenomena on other probes on the rear and leading cars could also be obtained. On similar positions stronger noise appears in the rear car, which is a result of strong turbulent flow there. For example, two strong vortices exist in the rear flow swirling in opposite directions as mentioned above. These characteristic structures are important noise sources in high speed trains. In order to efficiently reduce the aerodynamic noise, more reasonable streamline shape should be properly designed to suppress these vortices. Moreover, due to these vortices, acoustic surface should be longer than the train so as to contain all the noise sources.

4.5.4 Far field noise of high speed train

Currently far field aerodynamic noise is utilized as an important international standard to evaluate the noise level of high speed trains and normally the places which is 25m away and 3m high from the train are taken as observation points to record fluctuating data. In present work the far field observation points are selected just following the above standard, which are from P46 to P56 along the train. The A-weighted sound pressure levels of these probes are depicted in Fig 26 and frequency spectrum of specific probe is drawn in Fig. 27.

As seen in Fig. 27, the distribution of the noise levels for the far field probes is very uniform, mostly centralizing in the region between 77 dB(A) – 81 dB(A). The far field noise level is around 80 dB(A) when the high speed train runs at a speed of 300 km/h, which is a relatively low noise level and can meet the modern noise standard. Besides, the frequency spectrum of probe P46 is very similar to the probe P01 which is on the tip of the leading car. They both have a dominant frequency around 2000 Hz, and frequency modes exist in every 2000 Hz, which is a common feature for far field probes.

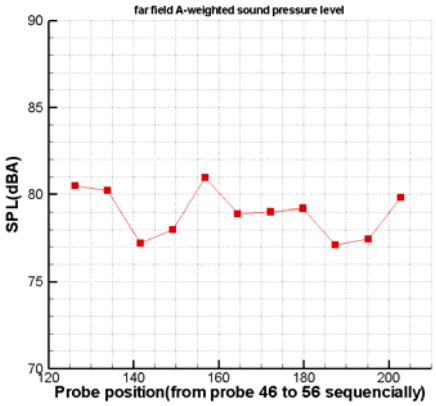

Fig. 26 Comparison of noise levels for far field probes.

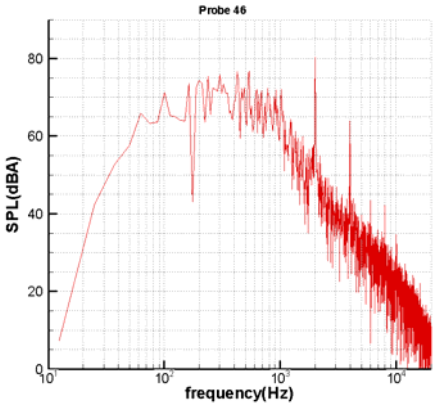

Fig. 27 Frequency spectrum of A-weighted sound pressure of P46.

5. CONCLUSIONS

Investigation on the aerodynamic noise in the near field and far field for the high speed train running at a speed of 300 km/h has been carried out, with the approach of NLAS and FW-H sound propagation equation adopted. A two-dimensional backward step case is chosen for method validation. Numerical results agree well with the experimental data, which ensures the suitability of the methods to be utilized in high speed train calculation.

Before the calculation of aerodynamic noise, a statistical steady RANS calculation is firstly performed and the characteristics of the steady flow field have been analyzed. Higher turbulence intensity exists on sides of the nose of the leading car. A vortex develops along the region between the nose and the fairing, and stretches along both sides of the body of the train. Strong disturbance arise when the vortex passes by, which would result in strong aerodynamic noise. A complex three-dimensional flow develops in the inter-coach spacing with a vortex stretching along the surface of the spacing. Compared to the flow

around the head of the leading car, the rear flow seems much more turbulent due to the disturbance of a blunt body, and develops two vortices swirling in opposite directions in the rear region.

With the help of probes at specific parts of the train, aerodynamic noise analysis of the high speed train has been performed. Results show that the head and the rear of the high speed train are main noise sources, and moreover the rear of the train is slightly higher than the head of the train in noise level at similar positions. The turbulence intensity of the boundary layer on the surface of the train is an important criterion to determine noise level. In general, higher turbulence intensity results in stronger noise. Uneven surfaces would increase the disorder in the boundary layer, which will produce stronger noise. As a result, the shoulder of the train, the flutes along the body and the nose of the leading and rear cars are all obvious noise sources. Due to the disturbance to the flow, the places where vortices pass by will generate strong noise too. For the flow in the inter-coach spacing, greater noise level exists in the trailing surface due to the interaction between the strong shear layer from the leading edge and the boundary layer on the trailing wall. In addition, the overall noise level of the rear power car is very high due to the unsteady flow structures in the rear flow. Study on the far field aerodynamic noise reveals that a noise level of 80 dB(A) could be maintained in the far field for the high speed train with a speed of 300 km/h, which could meet the modern noise standard.

ACKNOWLEDGEMENTS

The authors would like to thank Dr. Jie Zhang from Beijing Vision Strategy LTD for his great help. This work is supported by the National Science and Technology Pillar Program during the Eleventh Five-Year Plan Period (No.2009BAG12A01) and the National Key Basic Research and Development Program (973 program) (No.2011CB711101).

REFERENCES

1. Batten P, Goldberg U, Chakravarthy S (2002). Reconstructed sub-grid methods for acoustics predictions at all Reynolds numbers. *8th AIAA/CEAS Aeroacoustics Conference and Exhibit*.
2. Batten P, Ribaldone E, Casella M, Chakravarthy S (2004). Towards a generalized non-linear acoustics solver. *10th AIAA/CEAS Aeroacoustics Conferences*.
3. Casper J, Farassat F (2002a). A new time domain formulation for broadband noise predictions. *International Journal of Aeroacoustics* 1(3):207-240.
4. Casper J, Farassat F (2002b). Broadband noise predictions based on a new aeroacoustic formulation. *40th AIAA Aerospace Sciences Meeting and Exhibit*.
5. Curle N (1955). The influence of solid boundaries upon aerodynamic sound. *Proceedings of the Royal Society of London, Series A, Mathematical and Physical Sciences* 231(1187):505-514.
6. Fremion N, Vincent N, Jacob M, et al. (2000). Aerodynamic noise radiated by the inter-coach spacing and the bogie of a high speed train. *Journal of Sound and Vibration* 231(3):577-593.
7. Kalivoda M, Danneskiold-Samsoe U, Kruger F (2003). EURailNoise: A study of European priorities and strategies for railway noise abatement. *Journal of Sound and Vibration* 267(3):387-396.
8. Kitagawa T, Nagakura M (2000). Aerodynamic noise generated by Shinkansen cars. *Journal of Sound and vibration* 231(3):913-924.
9. Lee I, Sung HJ (2001). Characteristics of wall pressure fluctuations in separated and reattaching flows over a backward-facing step: Part 1. Time-mean statistics and cross-spectral analyses. *Experiments in Fluids* 30(3):262-272.
10. Lighthill MJ (1952). On sound generated aerodynamically: I general theory. *Proceedings of the Royal Society of London, Series A, Mathematical and Physical Sciences* 211(1107):564-587.
11. Lighthill MJ (1954). On sound generated aerodynamically: II turbulence as a source of sound. *Proceedings of the Royal Society of London, Series A, Mathematical and Physical Sciences* 222(1148):1-32.
12. Mellet C, Letourneaux F, Poisson F, Tallotte C (2006). High speed train noise emission: Latest investigation of the aerodynamic/ rolling noise contribution. *Journal of Sound and Vibration* 293(3-5):535-546.
13. Merci B, Vierendeels J, Langhe CD, Dick E (2001). Development and application of a new cubic low-Reynolds eddy-viscosity turbulence model. *31st AIAA Fluid Dynamics Conference & Exhibit*.

14. Moritoh Y, Zenda Y, Nagakura K (1996). Noise control of high speed Shinkansen. *Journal of Sound and Vibration* 193(1):319-334.
15. Nagakura K (2006). Localization of aerodynamic noise sources of Shinkansen trains. *Journal of Sound and Vibration* 293(3-5):547-556.
16. Noger C, Patrat JC, Peube J, Peube JL (2000). Aeroacoustical study of the TGV pantograph recess. *Journal of Sound and Vibration* 231(3):563-575.
17. Pronello C (2003). The measurement of train noise: a case study in northern Italy. *Transportation Research Part D* 8(2):113-128.
18. Sun ZX, Wang YW, An YR (2010). Computational study on aerodynamic sound from high-speed trains. *Journal of Hydrodynamics, Ser. A* 25(5):660-668 (in Chinese).
19. Talotte C (2000). Aerodynamic Noise: A critical survey. *Journal of Sound and Vibration* 231(3):549-562.
20. Talotte C, Gautier PE, Thompson DJ, Hanson C (2003). Identification, modeling and reduction potential of railway noise sources: A critical survey. *Journal of Sound and Vibration* 267(3):447-468.
21. Williams JEF, Hawkings DL (1969). Sound generation by turbulence and surfaces in arbitrary motion. *Philosophical Transactions for the Royal Society of London, Series A, Mathematical and Physical Sciences* 264(1151):321-342.